Response of a Cylindrical Shell to Random Acoustic Excitation

DANIEL D. KANA*
Southwest Research Institute, San Antonio, Texas

Response and equivalent force spectra have been investigated for random acoustic excitation of a cylindrical shell within a narrow frequency band of relatively low-modal density. Theoretical and experimental results are compared for single-point transfer functions, acoustic mobility functions, response and equivalent force power spectral densities, and coherence functions. In general, it is found that a purely theoretical prediction of response based on linear random process theory is severely limited because of the inability of currently available expressions for transfer functions to account for various deviations which result principally from imperfections and eccentricities in the cylinder. However, good agreement is achieved between measured response and that calculated with measured transfer functions. It is further indicated that a rather coarse discrete representation of a continuously distributed excitation is possible.

Nomenclature

a = shell radius
B_e = equivalent filter bandwidth for spectral density analysis
f = analysis frequency, Hz
h = thickness of shell wall
l = shell length
n_e = statistical degrees of freedom for spectral density analysis
RC = averaging time constant for spectral density analysis
ρ_s = shell mass density
ω = excitation circular frequency
ω_{mn} = natural frequency of m,nth mode

Introduction

DYNAMIC loading on launch and space vehicle structures is comprised to a great extent of spatially-distributed random acoustic energy that is generated by various sources within the vehicle environment. At launch, high-level engine noise is reflected from the ground up onto the structure, whereas during flight, aerodynamic turbulence as well as engine noise excite structural response. This response is important from the point of view of its influence on internal components and systems, in addition to that of structural integrity itself. Since cylindrical shells are a typical component in current structural designs, it is particularly important that their response to such distributed loads be understood.

A general analytical approach to determine the response of elastic structures to distributed random excitation has been given by Robson[1] as well as others. The essence of this approach involves first the determination of theoretical structural admittances or transfer functions between response at some appropriate point and harmonic excitation at a single point. These functions can conveniently be expressed as series expansions of the normal modes of the system. Then, by means of generalized harmonic analysis and superposition properties of linear random process theory, expressions are obtained which relate statistical properties of the response to the transfer functions and statistical properties of the excitation over the aggregate of points in the area over which a distributed load acts. This approach has been applied to the case of certain types of random response of a cylindrical shell by Nemat-Nasser,[2] and more recently by Hwang.[3] It is very evident from these analyses that the particular form of damping mechanism that is assumed has a profound influence on the response, as it does in any forced-vibration problem. It is further apparent that no modal distortions, and thereby deviations in response distributions, such as may be caused by eccentricities in the cylinder, can be predicted by such a theory.

In view of the fact that previous investigations[4] of dynamic shell behavior under harmonic excitation have uncovered various deviations of response from that predicted by normal modal theories, an experimental program was conducted to determine the validity of such theories as applied to the case of random excitation as well as to investigate several concepts important to the design of environmental tests for internal systems which may be attached to the shell. The results of this work are presented herein. For convenience, first a discussion of appropriate analytical relationships between excitation and response are given for the cylindrical shell. These are presented in a form for synthesizing a continuously distributed load into a gridwork of multiple discrete loads, so that information on the required mesh density for such a procedure can be obtained. Then, expressions are given for replacing the distributed load by an equivalent concentrated random load acting at the response point. Both of these concepts are of eminent importance in the design of force spectra for environmental testing of internal systems.

Analytical Expressions

Response to Multiple Discrete Excitation

It will be of convenience to decompose a continuously distributed random acoustical load into an aggregate of multiple discrete loads. For such a representation in a linearly elastic structure, the following matrix relationship can be written[5] between excitation and response:

$$S_{yy}(f) = (H_{xy})[S_{xx}]\{H_{xy}^*\} \quad (1)$$

where $S_{yy}(f)$ = displacement power spectral density of the response at y; (H_{xy}) = row vector of displacement admittance at y to force applied at x; $[S_{xx}]$ = square matrix of cross-spectral densities of excitation forces at various discrete points; and $\{H_{xy}^*\}$ = column vector of complex conjugates of elements of (H_{xy}).

Received February 9, 1970; revision received July 24, 1970. The results presented in this paper were obtained during the course of research sponsored by NASA Marshall Space Flight Center under Contract NAS8-21479. The author wishes to express his sincere appreciation to T. Dunham and D. Scheidt for aiding with the experiments, to W-H. Chu for theoretical discussions, and to R. Gonzales for digital computer programing.

* Senior Research Engineer (Group Leader), Department of Mechanical Sciences. Member AIAA.

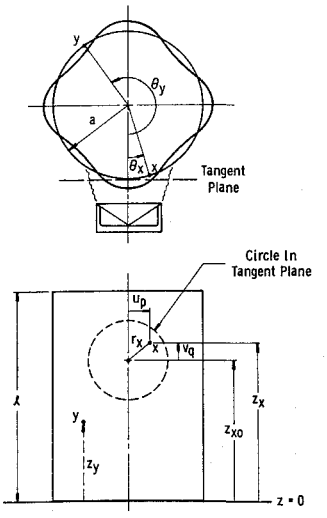

Fig. 1 Coordinate system.

The use of any transfer function in Eq. (1) is valid; here, however, displacement is chosen merely for convenience. For a purely theoretical application of this equation, analytical expressions must be utilized for the admittance functions. Analogous to section 4.7 of Robson,[1] for a cylindrical shell with coordinate system as indicated in Fig. 1, the following displacement admittance between a lateral excitation at x and displacement at y can be obtained:

$$H_{xy} = \sum_m \sum_n \frac{w_{mn}(z_y,\theta_y - \theta_x)w_{mn}(z_x,\theta_x = 0)(1 - \zeta^2 - i\eta_{mn})}{M_{mn}\omega_{mn}^2[(1 - \zeta^2)^2 + \eta_{mn}^2]} \tag{2}$$

where $\zeta = \omega/\omega_{mn}$ and

$$M_{mn} = \rho_s h a \int_0^l \int_0^{2\pi} w_{mn}^2(z,\theta)dzd\theta$$

For a simply-supported cylinder

$$w_{mn}(z,\theta) = \sin(m\pi z/l)\cos n\theta \tag{3}$$

so that

$$M_{mn} = \rho_s h a \pi l/2$$

It should be noted that a structural type of damping has been specified, and that the response pattern is assumed to follow the point x of load application, so that

$$w_{mn}(z_x,\theta_x) = \sin(m\pi z_x/l) \tag{4a}$$

$$w_{mn}(z_y,\theta_y - \theta_x) = \sin(m\pi z_y/l)\cos n(\theta_y - \theta_x) \tag{4b}$$

The latter behavior occurs in a perfectly symmetrical cylinder.

Equivalent Force Spectra

In order to determine the power spectral density of a single excitation force acting at point y in such a way as to replace the effects of the distributed or multiple discrete load, and to allow for the additional reaction effects of an internal system package, it is first necessary to develop several admittance relationships. Assuming steady-state harmonic excitation and response, we introduce the following notation: $F_y(f)$ = amplitude of applied excitation at y; $G_y(f)$ = amplitude of reaction force of internal system at y; $W_y(f)$ = displacement of shell at y when internal system is attached; $W_{yF}(f)$ = displacement of shell at y due to force $F_y(f)$ when internal system is detached; $W_{yG}(f)$ = displacement of shell at y due to the action of $G_y(f)$ alone; $H_{II}(f)$ = driving-point admittance of internal system; and $H_{yy}(f)$ = driving-point admittance at point y of shell only with internal system detached.

The complex admittance functions may be defined as having zero phase angle when displacement and force act in the same direction. Thus, for the cylinder and attached internal system we can write

$$W_y(f) = W_{yF}(f) + W_{yG}(f) \tag{5}$$

but

$$W_{yF}(f) = H_{yy}(f)F_y(f) \tag{6a}$$

$$W_{yG}(f) = -H_{yy}(f)G_y(f) \tag{6b}$$

and

$$G_y(f) = W_y(f)/H_{II}(f) \tag{6c}$$

Upon substitution of Eqs. (6) into Eq. (5) and solving for $G_y(f)$, there results

$$G_y(f) = F_y(f)H_{yy}(f)/[H_{yy}(f) + H_{II}(f)] \tag{7}$$

These expressions are valid for steady-state harmonic excitation. For the case of random excitation, by means of generalized spectral analysis,[5] Eqs. (6a) and (7) become

$$S_F(f) = |H_{yy}|^{-2}S_{yy}(f) \tag{8a}$$

$$S_G(f) = |H_{yy}(f)/[H_{yy}(f) + H_{II}(f)]|^2 S_F(f) \tag{8b}$$

It can be seen from Eqs. (8a) and (1) that $S_F(f)$ is an equivalent concentrated force spectra which acts at y in such a way as to produce the same response $S_{yy}(f)$ of the shell alone as that of a distributed load. Further, $S_G(f)$ is the force spectra to which the internal system alone must be subjected in order to duplicate the environment it must withstand as a result of the action of the distributed load on the shell. Finally, it should be recognized that idealized point contact at y has been assumed. That is, only lateral reactive force $G_y(f)$ has been considered, with other possible force components and rotations being neglected.

Experimental Procedures and Results

Measurement of Excitation Field

In order to employ Eq. (1) for prediction of shell response, it is necessary to determine the elements of the matrix $[S_{xx}]$ for a given distributed load. That is, the properties of the acoustic excitation field must be measured. For this purpose, a microphone was mounted in a simulated cylindrical section and placed in the same position relative to the acoustical speaker as that to be used when exciting the actual cylinder. Both the cylindrical section and the cylinder had the same radius. A photograph of this part of the apparatus is shown in Fig. 2. The microphone and section could be moved

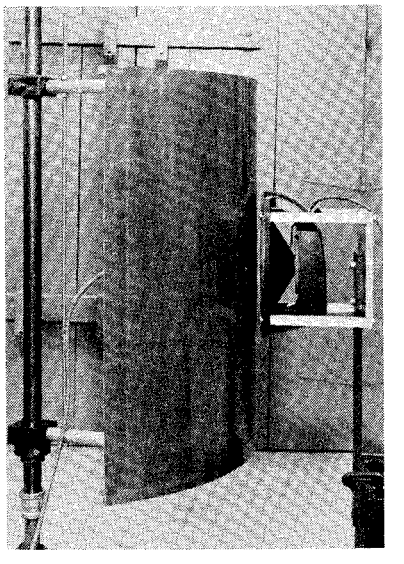

Fig. 2 Appartus for measuring acoustic field.

vertically and swung horizontally, whereas the speaker was driven by a Gaussian noise generator.

Thus, the speaker output was measured over its entire effective field and recorded on analog tape. The subsequent data were then processed by means of analog spectral analysis equipment in order to determine their statistical properties. Samples of the CO-spectrum between the acoustic pressure at the speaker centerline and other off-center positions are shown in Fig. 3 for a limited frequency band. The QUAD-spectrum, or the imaginary part of the ordinarily complex functions, was found to be essentially zero. These data show that, as a result of the low-frequency range and near proximity of speaker and shell, the imaginary part of the convective excitation field could be neglected. Further, the field was symmetrical and the elements of $[S_{xx}]$ were

$$S_{xx}(f) = k_x^2 S_{00}(f) \tag{9a}$$

$$S_{x_1x_2}(f) = S_{x_1x_2}(f) = k_{x_1}k_{x_2}S_{00}(f) \tag{9b}$$

where

$$k_x = e^{-[(r_x^{2.682})/28.8]} \tag{10}$$

and r_x is the radial distance off the speaker axis in a plane tangent to the cylinder as shown in Fig. 1. Further, $S_{00}(f)$ is the force PSD of the excitation at the point of intersection of the speaker centerline with the tank wall. Equation (10) is an empirical relationship which has been fit to the experimental data as shown in Fig. 4. This is a special case of the more general directly correlated field discussed on pp. 77–81 of Robson.[1] For this case, Eq. (1) reduces to

$$S_{yy}(f) = |\bar{\alpha}_{xy}|^2 \bar{S}_{00}(f) \tag{11}$$

where

$$\bar{\alpha}_{xy} = \Delta^2 \sum_p^N \sum_q^N k_x(p,q) H_{xy}(p,q) \tag{12}$$

is defined as an acoustical mobility function, Δ is the gridwork mesh size, and $\bar{S}_{00}(f)$ is the pressure power spectral density at the intersection of the centerline of the speaker with the shell (note $u_p = p\Delta$, $v_q = q\Delta$).

For later calculations, it was determined from Fig. 3 that at $(u_p,v_q) = (0,0)$ we have

$$\bar{S}_{00}(f) = 3.66 \times 10^{-7} \text{ psi}^2/\text{Hz}$$

as an average value throughout the frequency range of 100–180 Hz. Further, for single-point excitation to be described later, the same taped signal was utilized to drive a point-attached electrodynamic coil at a value of

$$S_{00}(f) = 1.26 \times 10^{-5} \text{ lb}^2/\text{Hz}$$

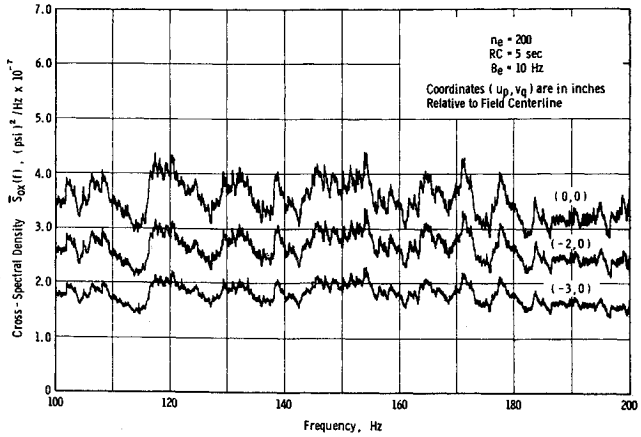

Fig. 3 Cross-spectral densities of acoustic field.

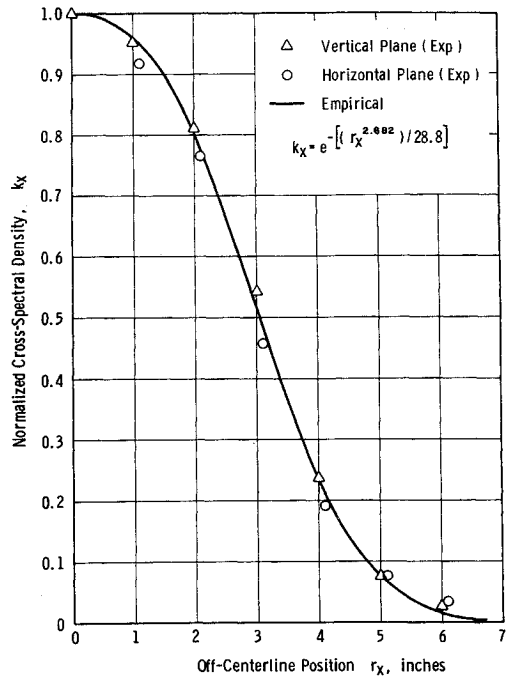

Fig. 4 Spatial distribution of acoustic field.

Harmonic Excitation and Response

Experiments with harmonic excitation of a cylinder were conducted both with single-point and distributed acoustic excitation in order to measure transfer (or admittance) functions and to observe the qualitative behavior of the system. The apparatus for single-point excitation is shown in Fig. 5. The electrodynamic shaker has a moving element of only 8 g, which is attached to the cylinder. Thus, mass loading effects were negligible in the frequency range of interest. A noncontacting Bentley transducer was used for measuring displacement (not shown in the photograph). The cylinder is attached to the end skirts primarily for ease in handling, and the combination is bolted to a solid closed base as shown, but is open at the top.

The cylinder shown in Fig. 5 is the same as that used in a previous study,[4] except that no bulkheads were incorporated for the present experiments. Properties of this cylinder along with some experimentally measured natural frequencies are given in Table 1. Damping factors η_{mn} were determined by measuring the transfer function for harmonic single-point excitation at the various natural frequencies and observing the displacement with the following parameters: $\theta_x = 0°$; $\theta_y = 180°$; $z_x = 15$ in.; and $z_y = 12.5$ in. The measured force and displacements were then substituted

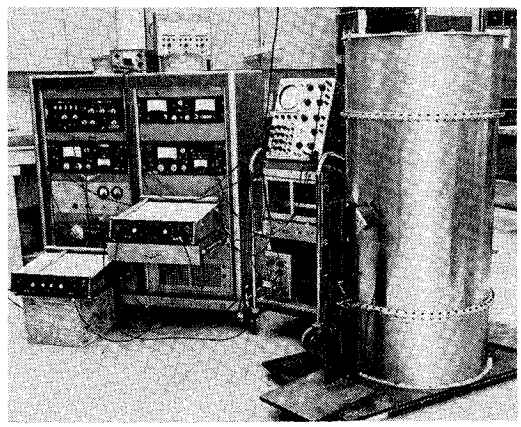

Fig. 5 Apparatus for point excitation of cylinder.

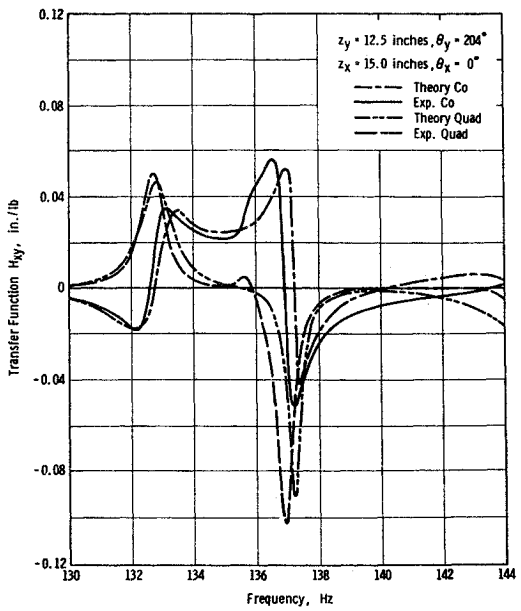

Fig. 6 Transfer function between Y1 and x = (0,0).

into Eq. (2), so that the various η_{mn} could be calculated. The summations in Eq. (2) were neglected for this purpose. This simplification is valid only for well separated modes and low damping. It is obvious from Table 1 that the damping factors are dependent on frequency, a result which is not predicted by simple structural damping theory.

Transfer functions were measured over a frequency band which included several of the lower-natural frequencies, and the results were compared with numerical results computed from Eq. (2), including the damping factors given in Table 1. The lowest nine modes were used for the series expression.

A comparison of results for one response point ($Y1$) and two-different excitation points is given in Figs. 6 and 7. Co and Quad refer, respectively, to the real and imaginary parts of the transfer function. It is obvious from the two figures that the modal pattern does indeed shift relative to the space-fixed coordinate system as the excitation point is moved around the circumference of the cylinder. However, discrepancies between theoretical and experimental results

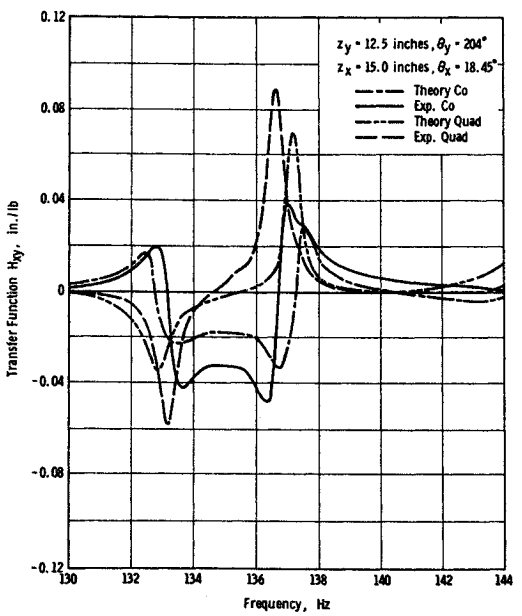

Fig. 7 Transfer function between Y1 and x = (4,0).

Table 1 Properties and natural frequencies of test cylinder

$\rho_s = 2.59 \times 10^{-4}$ lb sec²/in.⁴	$a = 12.42$ in.
$h = 0.020$ in.	$l = 30.0$ in.

Mode m	Mode n	Frequency Hz	Damping factor η_{mn}
1	5	214.7	0.00668
1	6	176.1	0.00922
1	7	144.5	0.01870
1	8	132.8	0.00977
1	9	137.2	0.00386
1	10	150.4	0.01380
1	11	168.0	0.01080
1	12	193.9	0.00531
1	13	224.8	0.00884
2	10	237.0	
2	11	241.0	
2	12	244.0	
2	13	259.0	

further indicate that some distortion of modal patterns also occurs. Nonalignment of peaks in the theoretical and experimental Quad part of the transfer functions indicates that slightly different resonant frequencies can be obtained by observing response at different points. Perfect alignment can be achieved only when the point of observation for experimental response is the same as that for which damping factors are calculated. This type of behavior results from eccentricities in the cylinder.

Distortion in modal response is even more apparent in Fig. 8 where a comparison in results is given for the acoustical mobility function between Y1 and harmonic acoustic excitation. Theoretical values are calculated from Eqs. (12, 2, and 10), along with a mesh size of $\Delta = \frac{1}{4}$ in. Except where stated otherwise, this mesh size was used for all subsequent results. The discrepancy in results evident in Fig. 8 indicates that distortion in response patterns are even more prevalent for distributed excitation. Further, evidence of split modes[6] is present and will be even more apparent in subsequent results.

A similar comparison between theoretical and experimental transfer and acoustic mobility functions is given in Figs. 9–11 for an additional observation point ($Y2$). The general behavior is similar to that previously described for ($Y1$).

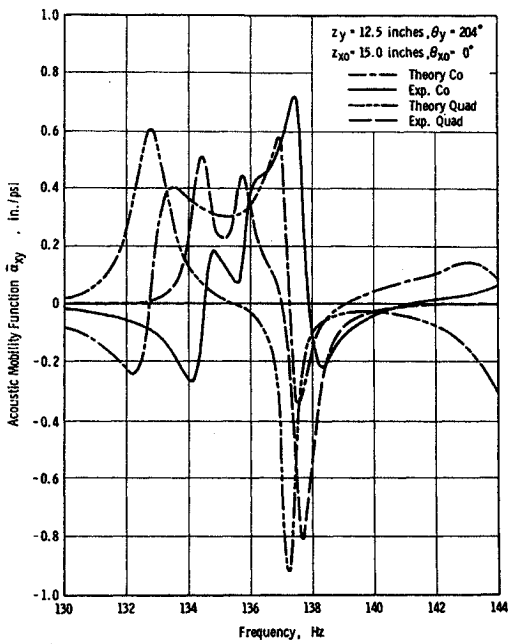

Fig. 8 Acoustic mobility function for Y1.

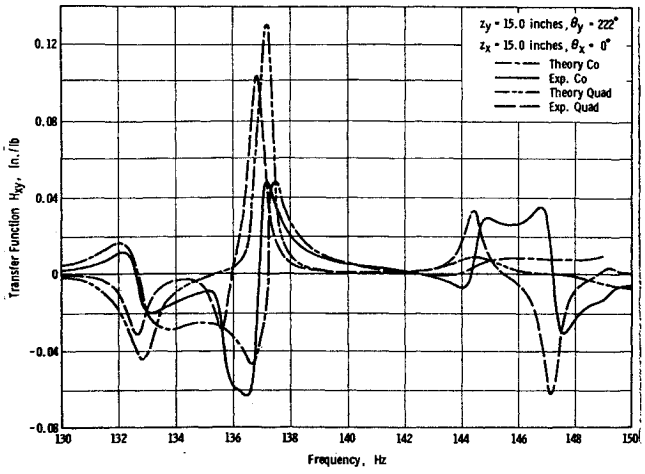

Fig. 9 Transfer function between $Y2$ and x = (0,0).

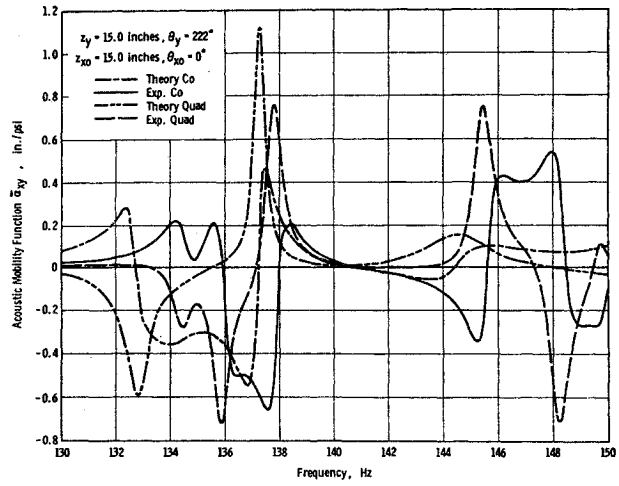

Fig. 11 Acoustic mobility function for $Y2$.

Random Excitation and Response

Responses to single-point and acoustic random excitation were determined at the same two observation points which were previously described. The same taped analog random signal whose properties were described in an earlier section was used to drive the cylinder for both types of excitation; whereas response data were simultaneously recorded on analog tape. Subsequent processing of the taped data was accomplished by analog analysis equipment. A speed factor increase of 32 was utilized in processing response data in order to allow an effective B_e = 0.312 Hz with a 10-Hz filter. Results are presented in Figs. 12 and 13, respectively. Theoretical results for single-point excitation are based on Eq. (11) in which $\bar{\alpha}_{xy}$ is replaced by a single theoretical transfer function H_{xy} between the response and excitation points, and $\bar{S}_{00}(f)$ is replaced by $S_{00}(f)$, the input force PSD for this case. Theoretical results for acoustic excitation are based directly on Eq. (11), including the appropriate theoretical expressions which make up $\bar{\alpha}_{xy}$ as given by Eq. (12). Average values for $\bar{S}_{00}(f)$ and $S_{00}(f)$ were taken as given in a previous section. Semiexperimental values of response are based on a procedure originated by Trubert.[7] That is, the response values are calculated by means of Eq. (11), except that experimentally measured, rather than theoretical, transfer functions or acoustic mobility functions are used as appropriate. For point $Y1$, these experimental functions have been given in Figs. 6 and 8.

It is obvious from Figs. 12 and 13 that considerable discrepancy exists between purely theoretical and experimental results. This is not surprising in view of similar discrepancies encountered for the transfer functions. However, it is equally obvious that except for some very slight shift in peak frequencies, quite good comparison is achieved between semiexperimental and experimental results. This indicates that the basic linear random process theory is applicable, so long as good representation of the transfer and acoustic mobility functions can be achieved.

In comparing Figs. 12 and 13, it can be seen that a partially split mode occurs for the acoustical input between 136 and 138 Hz, and similar peak responses occur for slightly different frequencies for the two different kinds of excitation. Such split resonances are even more apparent in Fig. 14 where additional response results are given for observation point $Y2$.

Equivalent force spectra for both points $Y1$ and $Y2$ are presented in Fig. 15 for purely theoretical data only. The results are based on Eqs. (8a) and (2). More accurate values would be obtained by using purely experimental values in the right side of Eq. (8a). However, the given results are sufficient to indicate the complexity of force spectral density which would be required to simulate the environment. Such complex force spectra are difficult to achieve with present-day electro-dynamic shaker equalization equipment.

The influence of mesh size on the theoretical results is indicated in Fig. 16 for one-typical frequency and observation point $Y1$. The results are normalized to that for a mesh

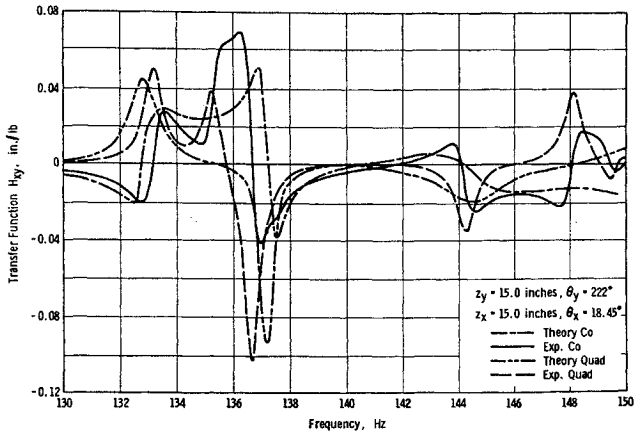

Fig. 10 Transfer function between $Y2$ and x = (4,0).

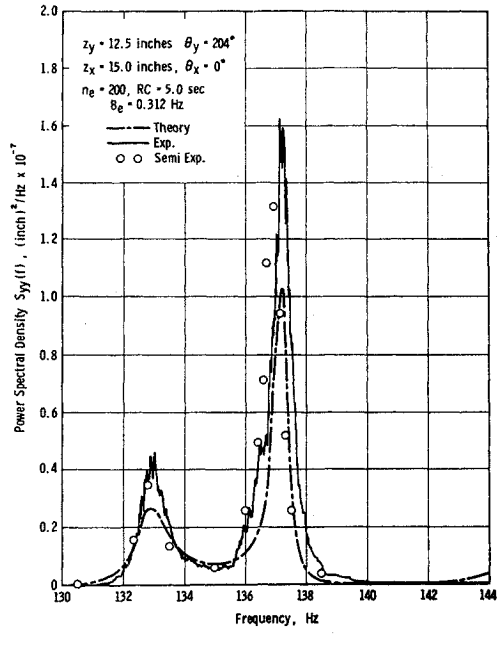

Fig. 12 Single point random response for $Y1$.

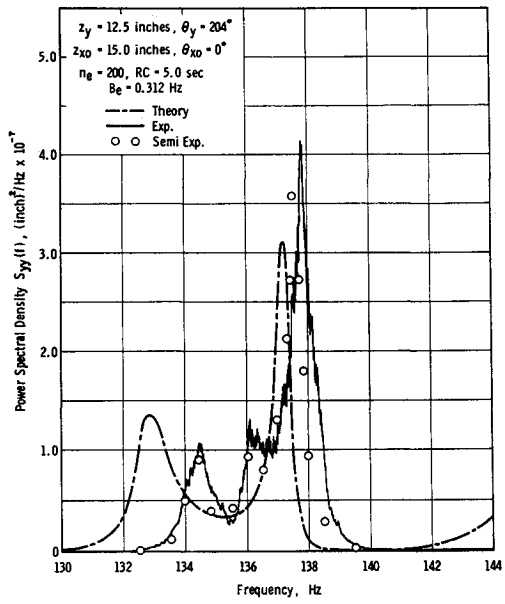

Fig. 13 Acoustic random response for Y1.

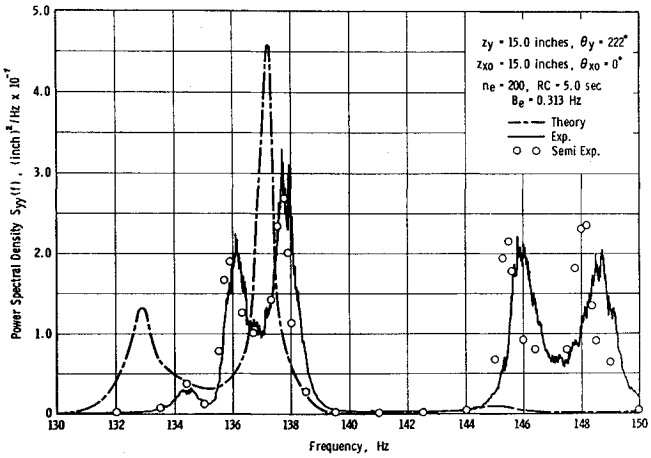

Fig. 14 Acoustic random response for Y2.

size of $\Delta = \frac{1}{4}$ in., which requires 2304-mesh points. The ratio Δ/L is that of mesh size to wave length for the dominant mode of response present, while $\Delta/r_{\max}$ is mesh size to maximum r_x, which from Fig. 4 was taken as 6 in. It is very interesting that equally valid results can be achieved with a mesh size as coarse as $\Delta = 2$ in. which requires only 144-mesh points.

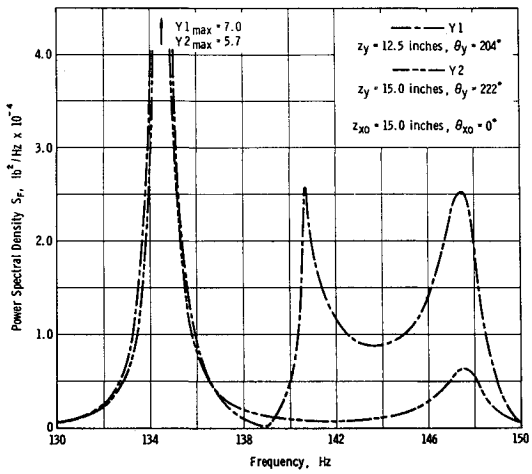

Fig. 15 Theoretical equivalent force spectra for Y1 and Y2.

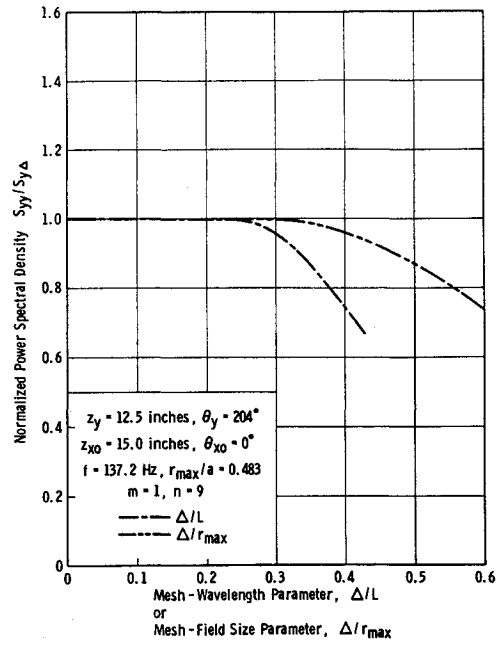

Fig. 16 Variation of acoustic response at Y1 with excitation mesh size.

The dependence of this trend on frequency and dominant modal pattern remains to be determined.

A final correlation of purely experimental data is presented in Fig. 17, where the ordinary coherence functions[5] have been calculated from $\gamma_{xy}^2 = |S_{0y}(f)|^2/[S_{yy}(f)S_{00}(f)]$ for single point excitation and $\gamma_{xy}^2 = |\bar{S}_{0y}(f)|^2/[S_{yy}(f)\bar{S}_{00}(f)]$ for acoustic excitation. In these expressions $S_{0y}(f)$ and $\bar{S}_{0y}(f)$ are the cross-spectral density measured between the response at y and, respectively, the force and pressure at $r_x = 0$. These functions should have a value near unity for a perfectly linear system and will be less than unity otherwise. However, they are highly sensitive to small deviations, and often a value of $\gamma_{xy}^2 \geq 0.6$ is a fair indication of linearity. It should be mentioned that for the acoustical input, an ordinary coherence value near unity is not necessarily an indication of linearity. However, as shown in the Appendix, it does provide such an indication in the present case where the excitation field is of the special convective form. In general, from Fig. 17 it can be concluded that excellent linearity is indicated for single point random excitation, whereas somewhat diminished linearity is suffered for acoustic random

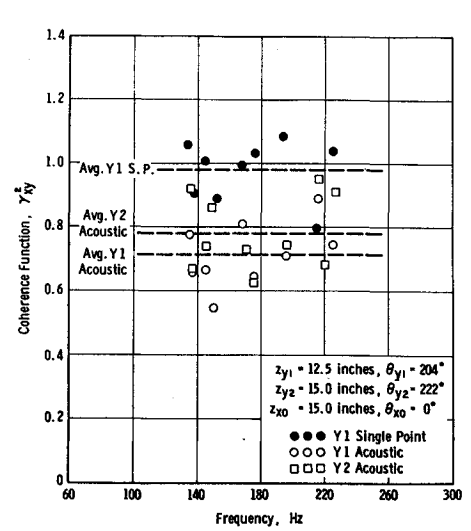

Fig. 17 Coherence function for random excitation.

excitation. These results appear generally to agree with the data previously presented.

Appendix

Ordinary Coherence Function for Perfectly Correlated Excitation Field

From Ref. 5,

$$\{S_{xy}(f)\} = [S_{xx}]\{H_{xy}\}$$

Let point $x = (0,0)$ be the excitation point for the first element of the column matrices in this expression. Then, in view of Eq. (9b), the first element of the left-hand matrix is

$$S_{0y}(f) = \sum_{i=1}^{N} S_{0i}H_{iy} = \sum_{i=1}^{N} k_{x_i}H_{iy}S_{00}(f)$$

Combining this result along with Eqs. (11) and (12), it is found that

$$\gamma_{0y}^2 = |\bar{S}_{0y}(f)|^2/[S_{yy}(f)\bar{S}_{00}(f)] = 1$$

The validity of this expression is a joint indication of the linearity of the system as well as an indication of the validity of Eq. (9b) for representing the experimental excitation field.

References

[1] Robson, J. D., *An Introduction to Random Vibration*, Elsevier Publishing Co., New York, 1964.

[2] Nemat-Nasser, S., "On the Response of Shallow Thin Shells to Random Excitations," *AIAA Journal*, Vol. 5, No. 7, July 1968, pp. 1327–1331.

[3] Hwang, C. and Pi, W. S. "Random Acoustic Response of a Cylindrical Shell," *AIAA Journal*, Vol. 7, No. 12, Dec. 1969, pp. 2204-2210.

[4] Kana, D. D. and Gormley, J. F., "Longitudinal Vibration of a Model Space Vehicle Propellant Tank," *Journal of Spacecraft and Rockets*, Vol. 4, No. 12, Dec. 1967, pp. 1585–1591.

[5] Bendat, J. S. and Piersol, A. G., *Measurement and Analysis of Random Data*, Wiley, New York, 1966.

[6] Tobias, S. A., "A Theory of Imperfection for the Vibration of Elastic Bodies of Revolution," *Engineering*, Vol. 172, 1951, pp. 409–411.

[7] Trubert, M. R. P., "Response of Elastic Structures to Statistically Correlated Multiple Random Excitations," *Journal of the Acoustical Society of America*, Vol. 35, No. 7, July 1963, pp. 1009–1022.

MARCH 1971 AIAA JOURNAL VOL. 9, NO. 3

A Theory of the High-Aspect-Ratio Jet Flap

KEITH P. KERNEY*
Cornell University, Ithaca, N. Y.

The method of matched asymptotic expansions, which Van Dyke used to formulate a lifting-line theory for high-aspect-ratio wings, is applied to a wing with jet flap. The development differs from Van Dyke's in that velocity components instead of the velocity potential are the dependent variables, thin-airfoil approximations are used throughout, and the jet flap is present. The theory is given for the case of a flat elliptic wing with spanwise-uniform jet-momentum coefficient and jet angle and the result is a simple equation for the lift coefficient. Comparison with the results of two earlier finite-aspect-ratio jet-flap theories shows close agreement. Certain approximations needed in the earlier theories to solve the integral equation for the upwash induced by a semi-infinite lifting surface are avoided by consistent use of the principle that, in the limit as the aspect ratio becomes infinite, the change in lift due to induced incidence is much smaller than the lift, so that the integral equation does not have to be solved.

I. Introduction

A JET flap is formed by a high-speed jet which emerges from a wing through a thin slit along its trailing edge. It affects the lift both by direct momentum reaction on the internal ducting and by changing the pressure distribution on the outer surface of the wing. Since this can increase the lift while most of the jet thrust is recovered as propulsion, the jet flap represents a way of combining the lifting and propulsive systems of jet aircraft.

An analytical model for a two-dimensional wing with jet flap has been developed by Spence[1,2] and others using the principles of thin-airfoil theory. The flows inside and outside the jet are assumed to be irrotational and at constant densities. The wing and jet are represented by vorticity bound to a semi-infinite line downstream of the leading edge on which mixed boundary conditions apply. The lift and pitching-moment coefficients for steady flow past an uncambered wing were calculated numerically in Ref. 1 and the lift coefficient was calculated analytically in Ref. 2. Erickson calculated the pitching-moment coefficient analytically in Ref. 3.

The three-dimensional analog of this jet-flap representation is a horseshoe-vortex system which lies in a semi-infinite strip of width equal to the wing span and with the bound segments of some of the vortices located downstream of the trailing edge. Theories developed by Maskell and Spence[4] and Hartunian[5] use the integral equation for the upwash induced by this vortex system and require certain approximations in order to make the equation tractable. The upwash far downstream—which must be known in order to calculate the lift coefficient—was found to be indeterminate

Received February 16, 1970; revision received June 29, 1970. This paper is based on part of a Ph.D. thesis. The advice and encouragement which W. R. Sears provided while the research reported here was being conducted are gratefully acknowledged. The research was partially supported by the U.S. Air Force Office of Scientific Research under contract number AF 49(638)-1346. The author is now at the Naval Ship Research and Development Center, Washington, D.C.

* Research Assistant. Member AIAA.